

A simplified view of blazars: why BL Lacertae is actually a quasar in disguise

P. Padovani

European Southern Observatory, Karl-Schwarzschild-Str. 2, D-85748 Garching bei München, Germany

P. Giommi, G. Polenta^a, S. Turriziani, V. D'Elia^a

ASI Science Data Center, c/o ESRIN, via G. Galilei, I-00044 Frascati, Italy

S. Piranomonte

^a*INAF-Osservatorio Astronomico di Roma, via Frascati 33, I-00040 Monteporzio Catone, Italy*

We put forward a scenario where blazars are classified as flat-spectrum radio quasars, BL Lacs, low synchrotron, or high synchrotron peaked objects according to a varying combination of Doppler boosted radiation from the jet, emission from the accretion disk, the broad line region, and light from the host galaxy. We thoroughly test this new approach, which builds upon unified schemes, using Monte Carlo simulations and show that it can provide simple answers to a number of long-standing open issues. We also demonstrate that selection effects play a very important role in the diversity observed in radio and X-ray samples and in the correlation between luminosity and the peak frequency of the synchrotron power (the so-called “blazar sequence”). It turns out that sources so far classified as BL Lacs on the basis of their observed weak, or undetectable, emission lines are of two physically different classes: intrinsically weak-lined objects, more common in X-ray selected samples, and heavily diluted broad-lined sources, more frequent in radio selected samples, which explains some of the confusion in the literature.

1. INTRODUCTION

Blazars are radio loud active galactic nuclei (AGN) pointing their jets in the direction of the observer [6, 48]. While all blazars emit variable, non-thermal radiation across the entire electromagnetic spectrum, they come in two main subclasses, whose major difference is in their optical properties: 1) Flat Spectrum Radio Quasars (FSRQs), which show strong, broad emission lines in their optical spectrum, just like radio quiet quasars; and 2) BL Lacertae objects (BL Lacs), which are instead characterized by an optical spectrum, which at most shows weak emission lines, sometimes displays absorption features, and in some cases can be completely featureless. Historically, the separation between BL Lacs and FSRQs has been made at the (rather arbitrary) rest-frame equivalent width (EW) of 5 Å [44, 45]. However, no evidence for a bimodal distribution in the EW of the broad lines of radio quasars has ever been found and, on the contrary, radio-selected BL Lacs were shown to be, from the point of view of the emission line properties, very similar to FSRQs but with a stronger continuum [40]. Most BL Lacs selected in the X-ray band, on the other hand, had very weak, if any, emission lines, and, when studying the properties of the X-ray selected *Einstein* Medium Sensitivity Survey (EMSS) sample, another criterion to identify them, this time to separate them from galaxies, had to be introduced [45]. This was based on the Ca H&K break, a stellar absorption feature typically found in the spectra of elliptical galaxies. Given that its value in non-active ellipticals is ~ 50%, a maximum value of 25% was chosen to ensure the presence of a substantial non-thermal continuum superposed to the host galaxy spectrum [45]. This

was later revised to 40% [22, 25].

Blazar classification depends then on the details of their appearance in the optical band where they emit a mix of three types of radiation: 1) a non-thermal, jet-related, component; 2) thermal radiation coming from the accretion onto the supermassive black hole and from the broad line region (at least in most radio-selected sources); 3) light from the host (giant elliptical) galaxy. Figure 1 represents these three components as red, blue and orange lines, overlaid to the spectral energy distribution (SED) of four well-known blazars [20]. The strong non-thermal radiation, the only one that spans the entire electromagnetic spectrum, is composed of two basic parts forming two broad humps, the low-energy one attributed to synchrotron radiation, and the high-energy one, usually thought to be due to inverse Compton radiation [e.g. 2]. The peak of the synchrotron hump (ν_{peak}) can occur at different frequencies, ranging from about $\sim 3 \times 10^{12}$ Hz to over 10^{18} Hz (see 3C 273 or 3C 279 and MKN 501 in Fig. 1) reflecting the maximum energy at which particles can be accelerated [e.g. 20]. Blazars with rest-frame $\nu_{\text{peak}} < 10^{14}$ Hz are called Low Synchrotron Peaked (LSP) sources, while those with 10^{14} Hz $< \nu_{\text{peak}} < 10^{15}$ Hz and $\nu_{\text{peak}} > 10^{15}$ Hz are called Intermediate and High Synchrotron Peaked (ISP and HSP) sources, respectively [2]. These definitions extend the original division of BL Lacs into LBL and HBL sources [30]. An expanded version of the work presented here is given by [18].

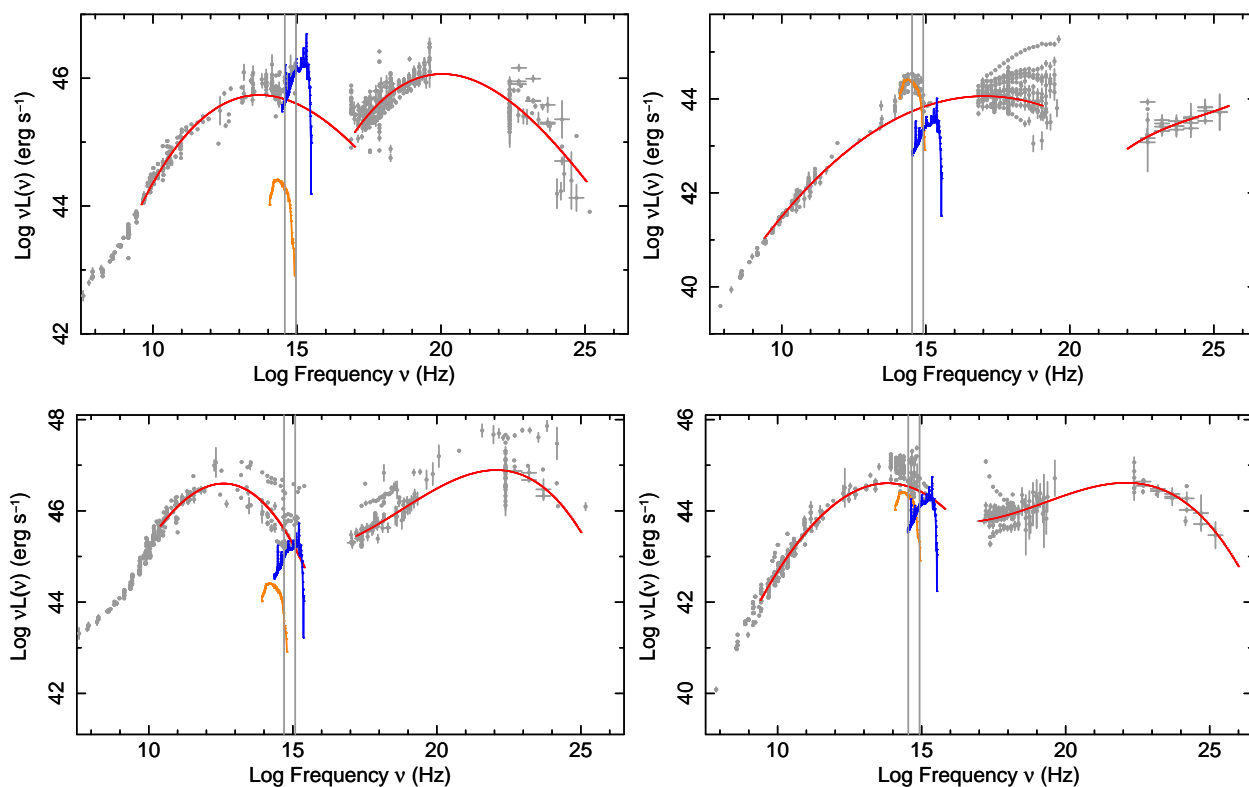


Figure 1: The SEDs of four representative blazars: two FSRQs, 3C 273 and 3C 279, and two BL Lacs, MKN 501 and BL Lac. The lines in color denote the three main components of blazars SEDs, namely non-thermal radiation from the jet (red), emission from the disk and from the broad line region represented by the composite QSO optical spectrum of [49] (blue), and light from the host galaxy, represented by the giant elliptical template of [24] (orange). The two vertical lines indicate the optical observing window (3800 – 8000 Å).

2. CURRENT STATUS

The two main blazar subclasses have many differences, which include:

1. *different optical spectra* (by definition). There are, however, a number of BL Lac - FSRQ transition objects, which include even BL Lacertae itself, the prototype of the class, which displays at times moderately strong, broad lines [e.g. 50] and 3C 279, a well-studied FSRQ, which can appear nearly featureless in a bright state [34];
2. *different extended radio powers*. Most BL Lacs have extended radio powers and morphologies consistent with those of Fanaroff-Riley (FR) type I, while basically all FSRQs are FR II-like [48, and references therein]. However, some radio-selected BL Lacs are known to possess an FR II-like structure [e.g. 38];
3. *very different redshift distributions*. FSRQs, similarly to radio quiet QSOs, are typically found at redshifts $\sim 1 - 2$, and up to ~ 5.5 , while BL Lacs are usually much closer with very few cases at $z \gtrsim 0.6$ [27]. A large fraction

of BL Lacs, however, [$\sim 43\%$ in BZCAT and $> 50 - 60\%$ of the BL Lacs in the Fermi 1 and 2 year AGN catalogs: 1, 3] have no measured redshift, due to the lack of any detectable feature in their optical spectrum, despite the use of 8/10-m class optical telescopes for the spectroscopy identification campaign;

4. *different cosmological evolutions*. Radio and X-ray selected samples have shown that the two blazar subclasses have very different cosmological evolutions, with FSRQs evolving strongly (again similarly to radio quiet QSOs) and BL Lacs evolving at a similar, or perhaps lower rate, in the radio band, or even showing no or negative evolution in the X-ray band [e.g. 31, 37, 44];
5. *widely different mix of FSRQs and BL Lacs in radio and X-ray selected samples*, with the latter typically including a much larger fraction of BL Lacs than the former. In fact, while only $\sim 15\%$ of WMAP5 blazars are BL Lacs (Section 3.1), this fraction is instead $\sim 70\%$ in the EMSS complete sample, which includes 41 BL Lacs and 15 FSRQs [33, 37];

6. *widely different distributions of the synchrotron peak energy ν_{peak} .* The rest-frame ν_{peak} distribution of FSRQs is strongly peaked at low energies ($\langle \nu_{\text{peak}} \rangle = 10^{13.1 \pm 0.1}$ Hz) and never reaches very high values ($\nu_{\text{peak}} \lesssim 10^{14.5}$ Hz) independently of the selection method [20], while the ν_{peak} distribution of BL Lacs is shifted to higher values by at least one order of magnitude. It can also reach values as high as $\nu_{\text{peak}} \gtrsim 10^{18}$ Hz and its shape varies strongly depending on the selection band [that is radio, X-ray or γ -ray: 2, 20].

Some of these differences have been explained by so-called unified schemes, which posit that BL Lacs and FSRQs are simply FR I and FR II radio galaxies with their jets forming a small angle with respect to the line of sight [48]. Radio galaxies would then be the “parent” population of blazars. Due to relativistic beaming this has enormous effects on their apparent emitted power and luminosity functions (LFs) and can explain their different extended radio powers and, partly, their cosmological evolutions. However, unified schemes per se cannot account for transition objects, the different evolution of radio and X-ray selected BL Lacs, and ν_{peak} distributions.

3. A NEW SCENARIO FOR BLAZARS

In our new scenario, the observed blazar optical spectrum is the result of a combination of an intrinsic EW distribution and the effects of three components: a non-thermal, jet related one, a thermal one due to the accretion disk, and emission from the host galaxy. Different mixes of these components determine the appearance of the optical spectrum and therefore the classification of sources in FSRQs (dominated by strong lines), BL Lacs (with diluted, weak lines, if a standard accretion disk is present), and radio-galaxies (where the host galaxy swamps both the thermal and non-thermal nuclear emission present in blazars). The other novel component is a single LF whose evolution depends on radio power.

3.1. Simulation ingredients

Our idea was tested through extensive Monte Carlo simulations, which include the following ingredients, which we kept as simple as possible and tied as much as possible to observational data:

1. **Luminosity function** We derive the LF and evolution of blazars at 41 GHz from the Wilkinson Microwave Anisotropy Probe (WMAP5) sample [52], which is practically equivalent to a radio-selected sample. We extend on the work of [16] and define a flux-limited sample of high Galactic latitude sources ($f_{41\text{GHz}} \geq 0.9$ Jy,

$|b_{\text{II}}| > 15^\circ$) including 161 FSRQs, 29 BL Lacs, and 10 blazars of unknown type. By applying a maximum likelihood technique to the WMAP5 blazars we obtain, together with the evolution discussed below, a best-fit local LF $\Phi(P) \propto P^{-3}$ (in units of $\text{Gpc}^{-3} \text{P}^{-1}$) between 1.9×10^{24} and 4.2×10^{27} W/Hz, which we assume in our radio simulations. Throughout this paper we use a Λ CDM cosmology with $H_0 = 70 \text{ km s}^{-1} \text{Mpc}^{-1}$, $\Omega_m = 0.27$ and $\Omega_\Lambda = 0.73$.

2. **Cosmological evolution** Powerful ($P_r \gtrsim 10^{26}$ W/Hz) radio sources display strong evolution at low redshifts followed by a decline at higher redshifts [e.g. 51]. We parametrize this behavior with a model of the type $P(z) = (1+z)^{k+\beta z}$, which allows for a maximum in the luminosity evolution followed by a decline. A maximum likelihood technique applied to the WMAP5 sample allows us to derive $k = 7.3$ and $\beta = -1.5$ in the $0 - 3.4$ redshift range (which implies a peak at $z \sim 1.85$), which we assume in our simulations. Lower luminosity ($P_r \lesssim 10^{26}$ W/Hz), mostly FR I radio sources display a much weaker cosmological evolution, which reaches \approx zero at $P_r < 10^{25}$ W/Hz [e.g. 12, and references therein]. We took this into account by using the radio LFs of BL Lacs and FSRQs derived from those of FR Is and FR IIs and based on the beaming model of [48]. We then used the fraction of beamed FR I blazars in bins of radio power to simulate the fraction of non-evolving radio sources as a function of power.

3. **Non-thermal component** To represent the non-thermal/jet component, we assume a simple homogeneous synchrotron self-Compton model [SSC, see, e.g. 47, and references therein] with relativistic electrons distributed as a power law at low energies and as a log-parabola at high energies [26]. This model represents well the synchrotron part of the observed SEDs, which always extends at least to the optical band where the classification of blazars as FSRQs or BL Lacs occurs. As for the inverse Compton emission, which can be important in the soft X-ray band, we set the Compton dominance so as to reproduce the observed f_x/f_r in FSRQs. The Lorentz factors of the electrons radiating at the peak of the synchrotron SED component (γ_{peak}) cover the range $\sim 10^{2.5} - 10^{4.5}$, which is that expected for typical parameters of the SSC model as shown in Fig. 36 of [2]. The shape of the distribution was chosen to reproduce the observed ν_{peak} distributions in radio and X-ray selected samples of blazars. We assumed a mean value of 15 for the Doppler factor δ . This was chosen to be consistent with the mean superluminal speed $\beta_{\text{app}} \sim 12$ obtained by [23], and with the typical

Lorentz factor $\Gamma \sim 15$ derived by [21] (since for the angle that maximizes the apparent velocity $\delta \sim \beta_{\text{app}} \sim \Gamma$).

4. Accretion Disk and broad emission lines

We use the quasar spectral template of [49] [see Fig. 4 of 20]. A standard accretion disk is likely to be present only in so-called “high excitation” radio galaxies (HERGs), while it appears not to be there, or be less efficient, in low-excitation ones (LERGs). Almost all FR Is are LERGs, while most FR IIs are HERGs, although there is a population of FR II LERGs as well. Observational evidence suggests that LERGs, which means all FR Is and some FR IIs, either do not possess an accretion disk, or if the disk is present is much less efficient than in FR IIs (i.e. of the Advection Dominated Accretion Flow [ADAF] type) [e.g. 10]. We have then associated the presence of a standard accretion disk only with beamed FR II sources and assumed that all those with an FR I parent (the non-evolving sources) have no disk.

5. Equivalent width distributions The intrinsic (before dilution) distributions of the EW of the broad lines ($\text{Ly}\alpha$, C IV, C III, Mg II, $\text{H}\beta$, $\text{H}\alpha$) have been assumed to be those of a sub-sample of the radio quiet QSOs included in the SDSS DR7 database (<http://www.sdss.org/dr7/>). We assumed Gaussian distributions characterized by the measured means ($\langle \text{EW}_{\text{H}\alpha} \rangle = 200 \text{ \AA}$, $\langle \text{EW}_{\text{H}\beta} \rangle = 23 \text{ \AA}$, $\langle \text{EW}_{\text{Mg-II}} \rangle = 18 \text{ \AA}$, $\langle \text{EW}_{\text{C-III}} \rangle = 16 \text{ \AA}$, $\langle \text{EW}_{\text{C-IV}} \rangle = 20 \text{ \AA}$, $\langle \text{EW}_{\text{Ly}\alpha} \rangle = 47 \text{ \AA}$) and dispersions for the various lines.

6. The disk to jet power ratio The disk and jet components in blazars are known to be correlated and possibly of the same order of magnitude [see, e.g. 8, 15]. We are interested in the somewhat simpler question of determining how the luminosity of the accretion disk (blue bump intensity at 5000 \AA) scales with radio power (at 5 GHz). The relevant data were derived by using the very large amount of multi-frequency information included in public databases and the tools that are now available to analyze SEDs [46]. Figure 1 gives some examples of representative objects. The amount of thermal flux in each FSRQ was estimated by matching the composite optical QSO spectrum of [49] to the SED data in the blazar rest-frame. Fig. 1 gives examples of the matching of the composite QSO spectrum (blue line) to the data for the case of 3C 273 or 3C 279. An upper limit was estimated for BL Lac objects by placing the composite QSO spectrum in the SED at an intensity such that the optical lines would not be

detectable in the optical spectrum (typically a factor ten below the observed flux. Fig. 1 illustrates the case of MKN501). This was done for the blazars selected in two surveys, WMAP5 and the EMSS. We found that $\alpha_{r-\text{BlueBump}}$ (the slope between the 5 GHz luminosity and the blue bump intensity at 5000 \AA and defined by $L_{\text{disk}} = L_{\text{r}}(\nu_{5000\text{\AA}}/\nu_{5\text{GHz}})^{-\alpha_{r-\text{BlueBump}}}$) correlates with radio luminosity, although with a large scatter. We then fitted a simple linear relationship between the two variables ($\alpha_{r-\text{BlueBump}} = 0.04 * \log(L_{\text{radio}}) - 0.39$) and assumed a Gaussian distribution around it with a dispersion of 0.1.

7. Host galaxy We have assumed that the host galaxy of blazars is a giant elliptical with fixed absolute magnitude of $M_{\text{R}} = -22.9$ [39, 41]. For the spectral shape we used the galaxy template of [24], who derived it combining the data from 28 local elliptical galaxies observed in the wavelength range 0.12 – 2.4 μm . Figure 1 shows this template superposed to the SED of four well-known blazars.

3.2. Simulation steps

Our Monte Carlo simulations start by drawing a random value for the radio luminosity and redshift based on the luminosity function and evolution described above and a value of the Lorentz factor of the electron radiating at the peak of the synchrotron power (γ_{peak}) from the assumed distribution. We then calculated the peak of the synchrotron power in the source rest frame by assuming a simple SSC model ($\nu_{\text{peak}} = 3.2 \times 10^6 \gamma_{\text{peak}}^2 B \delta$). The magnetic field was fixed to $B = 0.15$ Gauss and the Doppler factor δ was randomly drawn from a gaussian distribution with $\langle \delta \rangle = 15$ and $\sigma = 2$. We then calculated the observed radio flux density (from the radio luminosity and redshift) and the non-thermal emission in the optical and X-ray bands under the assumption that the spectral shape of the observed emission is a log parabola around ν_{peak} and that the low energy part of the SED (cm and mm wavelengths) is a power law (as is typically seen in blazars: see e.g. Fig. 1 for some representative examples). We then added an accretion (blue bump) component as described above (only for beamed FR II sources), re-scaling the SDSS quasar template to this value and drew a random value of the equivalent width of $\text{Ly}\alpha$, C IV, C III, Mg II, $\text{H}\beta$, $\text{H}\alpha$ starting from the EW distribution observed in the SDSS radio quiet QSOs. The host galaxy optical light was added assuming a standard giant elliptical and we then calculated the total optical light and the observed equivalent width of all the broad lines considered by taking into account the dilution due to the non-thermal and host galaxy optical light. Sources were classified as FSRQs if the rest-frame EW

of at least one of the broad lines that enter the optical band in the observer frame (which we assume to cover the 3,800 – 8,000 Å range) was > 5 Å. Otherwise, the object was classified as a BL Lac, unless the host galaxy dominated the optical light causing the Ca H&K break to be larger than 0.4 [22, 25], in which case the source was classified as a radio galaxy. A BL Lac whose maximum EW is < 2 Å, or for which the non-thermal light was at least a factor 10 larger than that of the host galaxy [35], was deemed to have a redshift which cannot be typically measured.

It is important to stress that the scope of our simulations is *not* to reproduce *all* the observational details. While that could be possible in theory, in practice it would require a large number of parameters and some speculations. Our approach is instead to keep the number of assumptions to a minimum, to obtain robust, almost model-independent conclusions.

We are confident that our main results are stable to changes in input parameters. The adopted LF and evolution were in fact varied by 1σ from the WMAP5 best fit and we also used as LF the sum of the BL Lac and FSRQ LFs based on the beaming model of [48]. We also run the simulations with values of $\langle\delta\rangle$ in the 5 to 20 range, and considering also a dependence of δ on radio power [e.g. 21]. No major changes were obtained as compared to our default assumptions.

3.3. Simulations of radio and X-ray surveys

We simulated a radio flux density limited survey with $f \geq 0.9$ Jy, to match the WMAP5 sample, and an X-ray flux limited survey down to 5×10^{-13} erg cm $^{-2}$ s $^{-1}$ in the 0.3 – 3.5 keV band, in order to be able to compare it with the EMSS. To ensure good statistics each simulation run included 10,000 sources. In the X-ray case, since radio powers reach lower values than in the radio case, we extrapolated the radio LF down to 1.9×10^{23} W/Hz assuming the same slope.

4. COMPARING SIMULATIONS AND REAL DATA

4.1. Radio flux density limited survey

Table I summarizes our main results by giving the number of sources per class, their mean redshift, and $\langle V/V_m \rangle$ (where V is the volume out to the source and V_m is the volume at the distance where the object would be at the flux limit: [42]). The number in parenthesis refers to the BL Lacs with measurable redshift, to which the mean redshift and $\langle V/V_m \rangle$ pertain. About 3/4 of our sources are classified as FSRQs, with the fraction of BL Lacs being $\sim 19.8\%$ of blazars, which is consistent with the value of $15.3^{+3.7}_{-3.0}\%$ in the

Table I Results from a simulation of a radio flux density limited survey (0.9 Jy)

Source type	Number	$\langle z \rangle$	$\langle V/V_m \rangle$
FSRQs	7,587	1.24	0.64
BL Lacs	1,879 (1,191)	0.87	0.60
Radio galaxies	534	0.04	0.48
Total	10,000	1.13	0.63

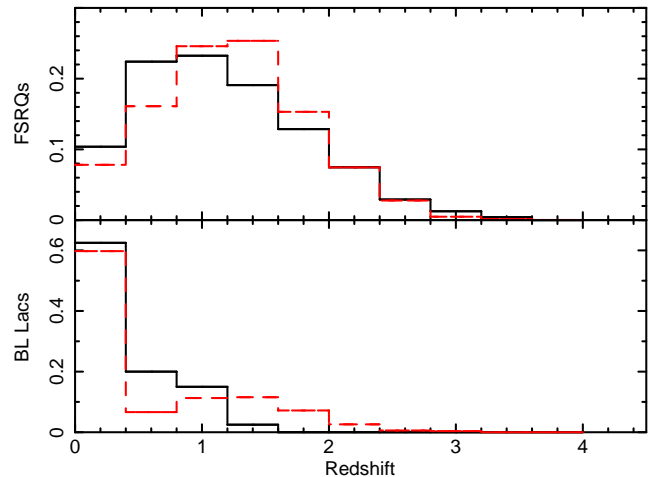


Figure 2: Top panel: the redshift distribution of the WMAP5 FSRQs (solid histogram) compared to that of FSRQs in a simulation of a radio survey (dashed histogram). Bottom panel: the redshift distribution of the WMAP5 BL Lacs (solid histogram) compared to that of BL Lacs in a simulation of a radio survey (dashed histogram)

WMAP5 sample. A small fraction (5%) of the simulated blazars are classified as radio galaxies. These are bona-fide blazars misclassified because their non-thermal radiation is not strong enough to dilute the host galaxy component. The mean redshift for our simulated FSRQs agrees with the WMAP5 value of 1.13, while for BL Lacs this is slightly larger than the WMAP5 mean (0.55). Fig. 2 shows the overall good agreement between our simulated redshift distributions (where we have only included sources with a measurable redshift) and the observed ones. 63% of our BL Lacs have a redshift determination, in excellent agreement with the WMAP5 value of $69^{+27}_{-20}\%$. 79% of the BL Lacs (68% of those with redshift) have a standard accretion disk and are therefore broad-lined but are classified as BL Lacs only because their observable emission lines are swamped by the non-thermal continuum. As regards $\langle V/V_m \rangle$, our simulated mean values agree with the observed ones of 0.62 ± 0.02 and 0.63 ± 0.05 for WMAP5 FSRQs and BL Lacs respectively [cf. also the value of 0.60 ± 0.05 for the 1 Jy BL Lac sample: 44]. Fig. 3 compares the distributions of ν_{peak} , the synchrotron peak en-

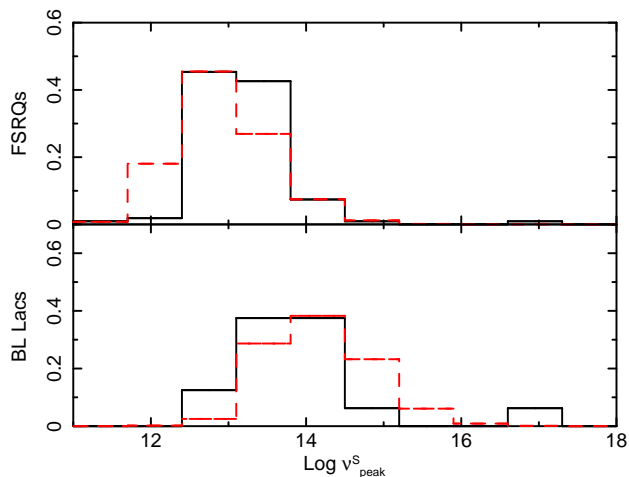


Figure 3: Top panel: the ν_{peak} distribution of radio selected FSRQs taken from the work of [20] (solid histogram) compared to that of FSRQs in a simulation of a radio survey (dashed histogram). Bottom panel: the ν_{peak} distribution of the BL Lacs in the radio sample of [20] (solid histogram) compared to that of BL Lacs in a simulation of a radio survey (dashed histogram).

Table II Results from a simulation of an X-ray flux limited survey (5×10^{-13} erg cm $^{-2}$ s $^{-1}$)

Source type	Number	$\langle z \rangle$	$\langle V/V_m \rangle$
FSRQs	2,836	1.23	0.65
BL Lacs (all)	5,622 (4,460)	0.36	0.51
BL Lacs ($\log \nu_{\text{peak}} > 16.5$)	927 (895)	0.33	0.45
BL Lacs ($\log \nu_{\text{peak}} > 17$)	185 (177)	0.34	0.34
Radio galaxies	1,542	0.04	0.48
Total	10,000	0.58	0.55

ergy, of sources classified as FSRQs and BL Lacs in our simulation with those of blazars included the radio sample of [20], which is the sample with the best determination of ν_{peak} values currently available. The agreement is clearly quite good and reproduces well the fact that BL Lacs tend to have ν_{peak} values significantly higher than FSRQs.

4.2. X-ray flux limited survey

Table II summarizes our main results. About 2/3 of our blazars are classified as BL Lacs, which is consistent with the value of $73^{+19}_{-15}\%$ in the EMSS sample. As in the radio case, a small fraction (15%) of the simulated blazars are misclassified as radio galaxies. The mean redshifts for our simulated FSRQs and BL Lacs are in reasonable agreement with the EMSS blazar sample values ~ 1 and ~ 0.37 . We note that, unlike the WMAP5 sample, the EMSS sample is relatively small (56 sources) and therefore a detailed comparison is hampered by the small number statistics. 79%

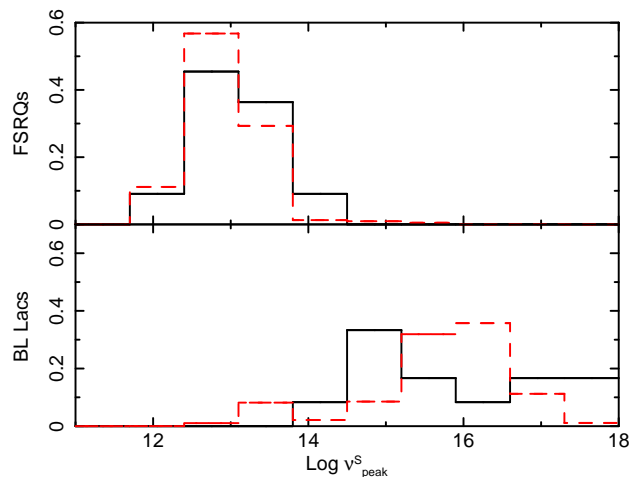


Figure 4: Top panel: the ν_{peak} distribution of the X-ray selected FSRQs in [20] (solid histogram) compared to that of FSRQs in a simulation of an X-ray survey (dashed histogram). Bottom panel: the ν_{peak} distribution of the BL Lacs in the X-ray flux limited sample of [20] (solid histogram) compared to that of BL Lacs in a simulation of an X-ray survey (dashed histogram).

of our BL Lacs have a redshift determination, in good agreement with the EMSS value of $93^{+26}_{-21}\%$. Although we assumed that all non-evolving sources do not have a standard accretion disk, 30% of the BL Lacs possess one and are classified as BL Lacs only because their emission lines are swamped by the non-thermal continuum. The smaller fraction of X-ray selected BL Lacs with disks in our simulations, as compared to radio-selected ones, is in accordance with the fact that fewer EMSS BL Lacs have emission lines clearly detectable in their optical spectra than, for example, 1 Jy BL Lacs [37, 38, 43]. As regards $\langle V/V_m \rangle$, our simulated mean values agree reasonably well with the EMSS ones of 0.67 ± 0.08 and 0.42 ± 0.05 for FSRQs and BL Lacs respectively, derived using the samples described in [33]. Fig. 4 compares the distributions of ν_{peak} of FSRQs and BL Lacs in our simulation with those of blazars belonging to the soft X-ray sample of [20], which includes *Planck*, *Swift* and *Fermi* observed blazars and it is therefore probably the sample with the best determination of ν_{peak} values currently available. Our simulations reproduce the fact that BL Lacs have much higher ν_{peak} values than FSRQs.

4.3. A blazar sequence?

The existence of an anti-correlation between bolometric luminosity and ν_{peak} , the “blazar sequence”, has been discussed since first proposed by [11] and [13] [e.g., 14, 17, 20, 28, 29, 33]. Figure 5 shows our radio and X-ray selected simulated blazars in the $\log(\nu_{\text{peak}}) - \log(\nu L_\nu(5 \text{ GHz}))$ plane. This reproduces the plot used by [11] to propose the existence of the

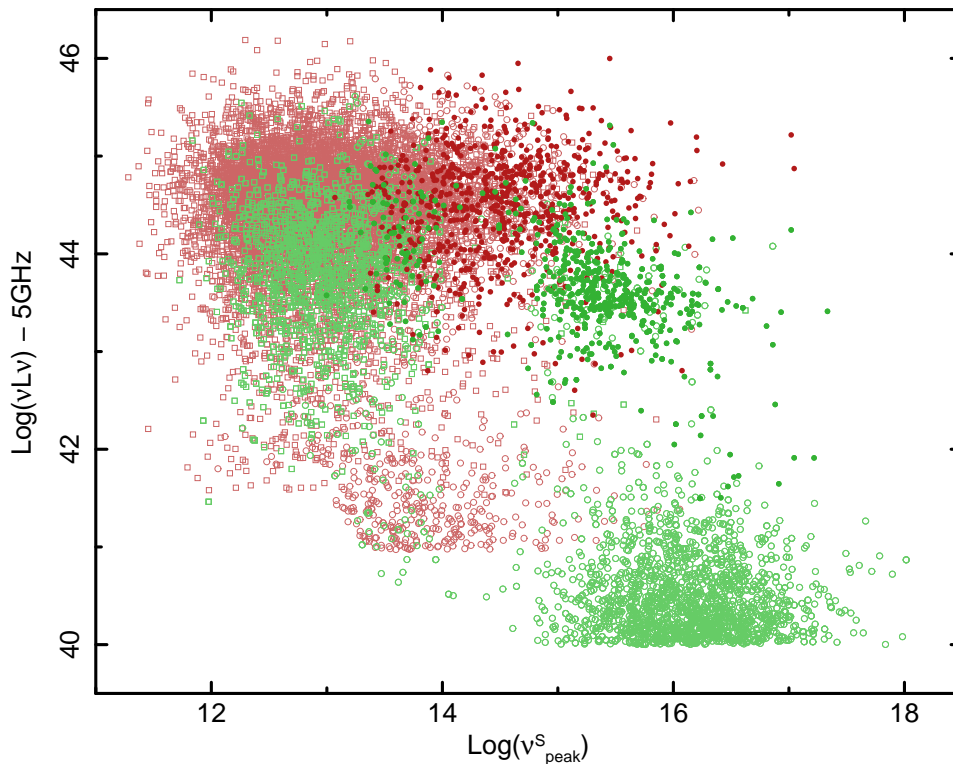


Figure 5: The FSRQs (open squares) and BL Lacs (circles) of our radio flux density limited ($f_r > 0.9$ Jy, red symbols) and X-ray flux limited ($f_x > 5 \times 10^{-13}$ erg cm $^{-2}$ s $^{-1}$, green symbols) simulated samples, plotted in the $\log(\nu)$ - $\log(\nu L_\nu)$ plane, the portion of the parameter space used by [11] to show the existence of the “blazar sequence” by comparing radio ($f_r > 1 - 2$ Jy) and X-ray selected ($f_x \gtrsim 10^{-12}$ erg cm $^{-2}$ s $^{-1}$) complete samples. Filled circles represent BL Lacs with very weak lines ($EW < 2$ Å) or completely featureless which, in a real survey would most probably not have a measured redshift, and therefore would not appear in the plot.

blazar sequence based on the correlation shown in this plane by FSRQs and BL Lacs discovered in shallow radio surveys (2 and 1 Jy samples) and BL Lacs found in the X-ray flux limited *Einstein* slew survey ($f_x \gtrsim 10^{-12}$ erg cm $^{-2}$ s $^{-1}$). Indeed, considered together the simulated radio and X-ray selected blazars display a broad correlation with radio selected FSRQs and BL Lacs (red open squares and open circles) mostly filling the top left and central part of the diagram and X-ray selected BL Lacs (green open circles) mostly confined to the lower right corner of the plot. This particular positioning of the points (bright FSRQs of the LSP type vs. fainter HSP BL Lacs) is not due to any intrinsic correlation between luminosity and ν_{peak} but results from the fact that bright radio sources are mostly drawn from the high end of the blazar luminosity function, while BL Lacs in X-ray flux limited samples are mostly high ν_{peak} sources (intrinsically rare) drawn from the low end of the luminosity function where the source density is largest. The most important difference between Fig. 5 and the diagram of [11] is in the high-luminosity - high ν_{peak} part, where most of the radio and X-ray selected objects with no redshift (red and green filled points) are located. These sources could not be plotted by

[11] since the luminosity of blazars without redshift cannot be estimated. This made the top right part of the [11] diagram empty, thus contributing to making the data points look like a sequence.

5. DISCUSSION

5.1. Evolution

A long-standing blazar puzzle is the difference in redshift distribution and cosmological evolution between FSRQs and BL Lacs, selected both in the radio and in the X-ray band. BL Lacs are mostly located at low redshifts and exhibit moderate, or even negative, evolution, while FSRQs evolve strongly just like radio quiet QSOs and show a redshift distribution that peaks at $z > 1$ [5, 16, 31, 37, 44]. Our simulations reproduce quite well both of these findings (see Fig. 2 and Tables I and II) implying that they are due to heavy selection effects. Most of the simulated BL Lacs found in radio surveys are luminous objects with broad lines that are diluted by non-thermal radiation beyond the 5 Å EW limit (many of them just below, thus allowing a measurement of their redshift), while

the BL Lacs found in simulated X-ray surveys typically show high ν_{peak} values (and therefore are X-ray bright) and are drawn from the low-power end of the radio luminosity function where non-evolving FR Is are preferentially found (Section 3.1). We note that the $\langle V/V_m \rangle$ of radio selected BL Lacs is not too different from that of FSRQs, while the $\langle V/V_m \rangle$ of X-ray selected BL Lacs is significantly lower, as found in real surveys (Section 4.1). Another interesting outcome of our simulations is the fact that X-ray selected BL Lacs with progressively larger values of ν_{peak} are characterized by lower and lower values of $\langle V/V_m \rangle$ (see Tab. II). This is in full agreement with the puzzling, and so far unexplained, results of [17] and [37] who reported that the $\langle V/V_m \rangle$ of BL Lacs is a function of their X-ray-to-radio flux ratio (which in turn depends on ν_{peak}).

5.2. ν_{peak} distribution

Recent results, based on radio and γ -ray surveys, have revealed that BL Lacs, on average, display a distribution of ν_{peak} energies, which is shifted to values higher than those of FSRQs [2, 20], expanding on the well-known fact that high ν_{peak} objects (HSPs) are always BL Lacs. This experimental difference is well reproduced in our simulations (see Fig. 3) which give $\langle \log(\nu_{\text{peak}}) \rangle = 12.9$ for FSRQs and $\langle \log(\nu_{\text{peak}}) \rangle = 14.1$ for BL Lacs for the case of a radio survey. This distinction is due to the fact that blazars with higher ν_{peak} values produce more non-thermal optical light than low ν_{peak} sources, diluting more easily the broad line component, and are therefore classified more frequently as BL Lac objects. We note that this has been interpreted in the literature as an intrinsic physical difference between LSP (detected mostly in the radio band) and HSP (detected mostly in the X-ray and γ -ray band) blazars due to the fact that HSPs are observationally characterized by a low intrinsic power and external radiation field, given their very weak or absent emission lines. As a consequence, cooling was thought to be less dramatic in HSP allowing particles to reach energies high enough to produce synchrotron emission well into the X-ray band [13]. In our scenario, instead, all sources have exactly the same chance of being HSP or LSP (that is, the value of γ_{peak} is drawn from a distribution independently of luminosity) and the very different ν_{peak} distributions observed in radio and X-ray surveys arise from the strong selection effect discussed in Section 4.3 and the emission line dilution mentioned above. Our simulations predict the existence of a significant number of BL Lacs with redshift that cannot be measured, which can occur when both ν_{peak} and radio power are so large that dilution becomes extreme. For example, $\sim 81\%$ of our simulated sources with $\nu_{\text{peak}} > 10^{15}$ Hz and $P_r > 10^{26}$ W/Hz have no redshift. This is consistent with the

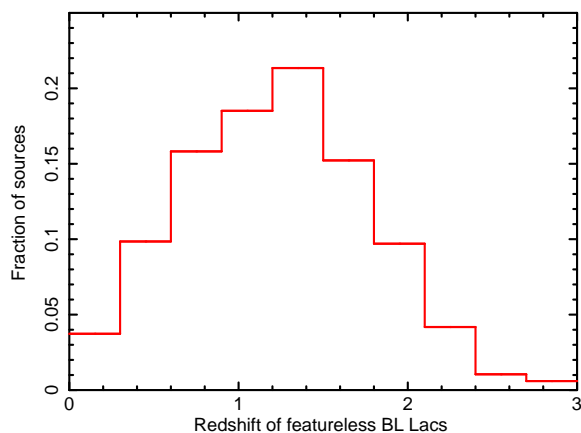


Figure 6: The redshift distribution of the BL Lacs that show a featureless spectrum in our simulation of a radio flux density limited survey and that in a real survey would have no redshift determination.

fact that most BL Lacs in current γ -ray selected samples have no measured redshift, as *Fermi* is known to preferentially select high ν_{peak} BL Lacs [1, 3]. This effect is also clearly shown in Fig. 5 where most of the simulated blazars with no measurable redshift (filled circles with light colors) occupy the top right part of the diagram. Fig. 6 shows the intrinsic redshift distribution of these featureless BL Lacs for the case of our simulation of a radio flux density limited survey.

5.3. What is a BL Lac?

It was originally suggested that the absence of broad lines in BL Lacs was due to a very strong, Doppler-boosted synchrotron continuum [6]. In the years following that paper observations of various BL Lacs, mostly selected in the X-ray band, showed that in many cases their optical spectrum was not swamped by a non-thermal component, as host galaxy features were very visible, and it was thought that most BL Lacs had intrinsically weak lines [45]. We have shown here that these two possibilities are not mutually exclusive and indeed are both viable, depending on radio power and, therefore, on the band of selection. One important consequence of our scenario is that objects so far classified as BL Lacs on the basis of their *observed* weak, or undetectable, emission lines belong to two physically different classes: intrinsically weak-lined objects, whose parents are LERGs/FR Is (more common in X-ray selected samples, since they reach lower radio powers) and heavily diluted broad-lined sources, which are beamed HERGs/FR IIs (more frequent in radio selected samples). Therefore, while the non-thermal engine is probably the same, the thermal one is obviously different. This solves at once the issue of the FSRQ/BL Lac transition objects and of the many differences between BL Lacs selected in the radio and X-ray bands, which include line strength,

extended radio emission and morphology, and evolution [e.g. 38, and references therein]. It also implies that BL Lacertae, the prototype of the class, is actually *not* a BL Lac but an FSRQ with its emission lines swamped by the jet. This hypothesis, which explains also many other open issues of blazar research, is testable. Our simulations, in fact, imply that the majority of sources in high-flux density radio-selected samples are identified as BL Lacs only because all lines have $EW < 5 \text{ \AA}$ in the optical observing window. These sources should show a strong ($EW > 5 \text{ \AA}$) H α line in the near or mid-infrared, since this is the strongest emission line, and would then be considered FSRQs. HERG/FR II BL Lacs, then, should be easily recognizable through infrared spectroscopy. These sources, as expected, are also more dominant at higher radio powers: for example, according to our radio simulation the fraction of BL Lacs with standard accretion disks is only $\sim 3\%$ for $P_r \leq 10^{26} \text{ W/Hz}$ but becomes $\sim 98\%$ above this value. This also means that fainter radio-selected samples of BL Lacs should be more and more similar to X-ray selected ones, apart from their ν_{peak} values, since higher ν_{peak} are easier to detect in the X-rays [30]. The implications of our hypothesis for unified schemes is quite straightforward: the parent population of BL Lacs need to include both LERGs/FR Is and HERGs/FR IIs, while that of FSRQs is made up of HERGs/FR IIs only. This should have only a small effect, for example, on the LF fitting done by [48], as HERG/FR II BL Lacs make up the high-power end of the radio LF while most of the number density comes from LERG/FR I BL Lacs.

5.4. Blazar classification

Our new scenario has strong implications on blazar classification. If the relevant physical distinction for radio sources is between LERGs (mostly FR Is) and HERGs (FR IIs), for most purposes then (LFs, evolution, etc.) HERG/FR II BL Lacs should be simply grouped with FSRQs. How does one distinguish in practice HERG/FR II BL Lacs from LERG/FR I BL Lacs? This is simple in the presence of *any* (even weak) broad lines or for transition objects. In other cases (e.g. completely featureless spectrum or in presence of absorption features) there is no easy way to distinguish between the two subclasses although, for example, radio power and/or morphology could help. Given the paucity of known LERG/FR Is at relative high redshifts, X-ray selected (and also fainter radio-selected) BL Lac samples are also useful in selecting such sources, which are very relevant also for the study of the so-called ‘‘AGN feedback’’ and the role that AGN radio emission plays in galaxy evolution through the so-called ‘‘radio-mode’’ accretion [7]. It should also be clear that BL Lacs can be used to study the broader issue of the relationship

between LERGs and HERGs, including their evolution. A by-product of our simulations has also been the realization that some sources classified as radio-galaxies do *not* have their jets oriented at large angles with respect to the line of sight, as expected, but are instead moderately beamed blazars with their non-thermal emission swamped by the galaxy (note that none of these objects has a standard accretion disk). These sources, which are all local ($\sim 90\%$ at $z \leq 0.07$) should be recognizable by their blazar-like SEDs and indeed some of them have already been identified by [9], [19] and [4]. Recently, a new classification scheme has been proposed to divide BL Lacs from FSRQs, which is based on the broad line region (BLR) luminosity in Eddington units and set at a dividing value of $L_{\text{BLR}}/L_{\text{Edd}} \sim 5 \times 10^{-4}$ [15]. This turns out to be also the value, which separates radiatively efficient (i.e., standard accretion disks) from radiatively inefficient (i.e., ADAFs) regimes, and therefore coincides with our HERG/FR II – LERG/FR I division. Therefore, [15] are also suggesting that HERG/FR II BL Lacs belong with the FSRQs.

6. TESTS AND PROSPECTS

Very recently, redshift constraints for 103 blazars from the *Fermi* 2LAC catalogue [3] have been derived by fitting SED templates to their UV-to-near-IR multi-band photometry obtained quasi-simultaneously with *Swift*/UVOT and GROND [36]. This was done using the attenuation due to neutral hydrogen along the line of sight at the Lyman limit to estimate the redshift of the absorber. Eleven of these objects have $z_{\text{phot}} > 1.2$. Some of us have studied the SEDs of these sources using quasi-simultaneous near-IR to X-ray data. Four blazars turned out to be of a type never seen before but with properties we were expecting for some of the BL Lacs without redshift: large ν_{peak} ($\sim 5 \times 10^{15} \text{ Hz}$) and high-power (see filled circles in Fig. 5) [32]. Given their featureless optical spectra, these sources are therefore most likely high-redshift FSRQs with their emission lines swamped by the jet, as predicted by our hypothesis.

In this paper we limited our simulations to the radio and the X-ray bands where SSC is a fair approximation of the observed non-thermal emission. The properties of γ -ray detected blazars are instead not consistent with simple SSC models [e.g. 2], and almost half of the radio and X-ray selected LSP blazars are γ -ray quiet [e.g. 20]. The present approach must therefore be integrated with additional information about the properties of the inverse Compton emission before it can be used to simulate γ -ray surveys. We are planning to extend our simulations to the γ -ray band by taking into account the recent results of [20] who determined the γ -ray properties of blazar samples selected in different bands.

Acknowledgments

We thank Matteo Perri for providing part of the software used for our Monte Carlo simulations. We acknowledge the use of data and software facilities from the ASI Science Data Center (ASDC), managed by the Italian Space Agency (ASI). Part of this work is based on archival data and on bibliographic information obtained from the NASA/IPAC Extragalactic Database (NED) and from the Astrophysics Data System (ADS).

References

- [1] Abdo A. A., et al., 2010a, *ApJ*, 715, 429
- [2] Abdo A. A., et al., 2010b, *ApJ*, 716, 30
- [3] Ackermann M., et al., 2011, *ApJ*, 743, 171
- [4] Antón S., Browne I. W. A., 2005, *MNRAS*, 356, 225
- [5] Beckmann V., Engels D., Bade N., Wucknitz O., 2003, *A&A*, 401, 927
- [6] Blandford R. D., Rees M. J., 1978, in *Pittsburg Conference on BL Lac Objects*, Ed. A. M. Wolfe, Pittsburgh, University of Pittsburgh press, p. 328
- [7] Croton D. J., et al., 2006, *MNRAS*, 365, 11
- [8] D’Elia V., Padovani P., Landt H., 2003, *MNRAS*, 339, 1081
- [9] Dennett-Thorpe J., Marchã M. J., 2000, *A&A*, 361, 480
- [10] Evans D. A., Worrall D. M., Hardcastle M. J., Kraft R. P., Birkinshaw M., 2006, *ApJ*, 642, 96
- [11] Fossati G., Maraschi L., Celotti A., Comastri A., Ghisellini G., 1998 *MNRAS*, 299, 433
- [12] Gendre M. A., Best P. N., Wall J. V., 2010, *MNRAS*, 450, 1719
- [13] Ghisellini G., Celotti A., Fossati G., Maraschi L., Comastri A., 1998, *MNRAS*, 301, 451
- [14] Ghisellini G., & Tavecchio F., 2008, *MNRAS*, 387, 1669
- [15] Ghisellini G., Tavecchio F., Foschini L., Ghirlanda G., 2011, *MNRAS*, 414, 2674
- [16] Giommi P., Colafrancesco S., Padovani P., Gasparri D., Cavazzuti E., Cutini S., 2009, *A&A*, 508, 107
- [17] Giommi P., Menna M.T., Padovani, P., 1999, *MNRAS*, 310, 465
- [18] Giommi P., Padovani, P., Polenta, G., Turriziani, S., D’Elia, V., Piranomonte, S., 2012, *MNRAS*, 420, 2899
- [19] Giommi P., Piranomonte, S., Perri, M., Padovani, P., 2005, *AA&A*, 434, 385
- [20] Giommi P., et al., 2011, *A&A*, in press (arXiv:1108.1114)
- [21] Hovatta T., Valtaoja E., Tornikoski M., Lähteenmäki A., 2009, *A&A*, 494, 527
- [22] Landt H., Padovani P., Giommi P., 2002, *MNRAS*, 336, 945
- [23] Lister M. L., et al., 2009, *AJ*, 138, 1874
- [24] Mannucci F., Basile F., Poggianti B. M., Cimatti A., Daddi E., Pozzetti L., Vanzi L., 2001, *MNRAS*, 326, 745
- [25] Marchã M. J. M., Browne I. W. A., Impey C. D., Smith P. S., 1996, *MNRAS*, 281, 425
- [26] Massaro E., Tramacere, A., Perri, M., Giommi, P., Tosti, G., 2006, *A&A*, 448, 861
- [27] Massaro E., Giommi P., Leto C., Marchegiani P., Maselli A., Perri M., Piranomonte S., Sclavi S., 2009, *A&A*, 495, 691
- [28] Nieppola E., Valatoja E., Tornikoski M., Hovatta T., Kotiranta M., 2008, *A&A*, 488, 867
- [29] Padovani P., 2007, *Ap&SS*, 309, 63
- [30] Padovani P., Giommi P., 1995, *ApJ*, 444, 567
- [31] Padovani P., Giommi P., Landt H., Perlman E. S., 2007, *ApJ*, 662, 198
- [32] Padovani P., Giommi P., Rau A., 2012, *MNRAS*, 422, L48
- [33] Padovani P., Perlman E. S., Landt H., Giommi P., Perri M., 2003, *ApJ*, 588, 128
- [34] Pian E., et al., 1999, *ApJ*, 521, 112
- [35] Piranomonte S., Perri M., Giommi P., Landt H., Padovani P., 2007, *A&A*, 470, 787
- [36] Rau A., et al., 2012, *A&A*, 538, A26
- [37] Rector T. A., Stocke J. T., Perlman E. S., Morris S. L., Gioia I. M., 2000, *AJ*, 120, 1626
- [38] Rector T. A., Stocke J. T., 2001, *AJ*, 122, 565
- [39] Sbarufatti B., Treves A., Falomo R., 2005, *ApJ*, 635, 173
- [40] Scarpa R., Falomo R., 1997, *A&A*, 325, 109
- [41] Scarpa R., Urry C. M., Falomo R., Pesce J. E., Treves A., 2000, *ApJ*, 532, 740
- [42] Schmidt M., 1968, *ApJ*, 151, 393
- [43] Stickel M., Fried J. W., Kühr H., 1993, *A&AS*, 98, 393
- [44] Stickel M., Padovani P., Urry C. M., Fried J. W., Kühr H., 1991, *ApJ*, 374, 431
- [45] Stocke J. T., Morris S. L., Gioia I. M., Maccacaro T., Schild R., Wolter A., Fleming T. A., Henry J. P., 1991, *ApJS*, 76, 813
- [46] Stratta G., Capalbi M., Giommi P., Primavera R., Cutini S., Gasparri D., 2011, arXiv:1103.0749
- [47] Tramacere A., Giommi P., Perri M., Verrecchia F., Tosti G., 2009, *A&A*, 501, 879
- [48] Urry C. M., Padovani P., 1995, *PASP*, 107, 803
- [49] Vanden Berk, D. E., et al., 2001, *AJ*, 122, 549
- [50] Vermeulen R. C., Taylor, G. B., Readhead A. C. S., Browne, I. W. A., *AJ*, 111, 1013
- [51] Wall J. V., Jackson C. A., Shaver P. A., Hook I. M., Kellermann K. I., 2005, *A&A*, 434, 133
- [52] Wright E. L., et al., 2009, *ApJS*, 180, 283